In situ measurements of the axial expansion of palladium microdisks during hydrogen exposure using diffraction phase microscopy

Chris Edwards,[1,2,4] Steven J. McKeown,[1,4] Jerry Zhou,[1,3] Gabriel Popescu,[2] and Lynford L. Goddard[1*]

[1]*Photonic Systems Laboratory, Department of Electrical and Computer Engineering, Micro and Nanotechnology Lab, University of Illinois at Urbana-Champaign, Urbana, Illinois 61801, USA*
[2]*Quantitative Light Imaging Laboratory, Department of Electrical and Computer Engineering, Beckman Institute for Advanced Science and Technology, University of Illinois at Urbana-Champaign, Urbana, Illinois 61801, USA*
[3]*Currently with the Department of Electrical Engineering and Computer Science, Massachusetts Institute of Technology, Cambridge, Massachusetts 02139, USA*
[4]*denotes equal contribution*
[*]*lgoddard@illinois.edu*

Abstract: We measured the height of Pd microdisks during H_2 exposure using epi-illumination diffraction phase microscopy, a quantitative phase imaging technique for capturing nanoscale dynamics in situ. From these microdisk height measurements, we extracted the axial expansion coefficient as a function of H_2 concentration as well as image sequences that show the instantaneous rate of axial expansion in a spatially and temporally resolved manner. Quantifying these two parameters is important in modeling Pd-based H_2 sensors. For H_2 concentrations below 0.5%, i.e. an order of magnitude below the lower explosive limit, the axial expansion coefficient followed the Freundlich distribution: $\Delta h(c) = 1.28\ c^{0.51}$ where Δh is the percentage change in height of the Pd microdisk and c is the percent concentration of H_2 in N_2. The fit agrees well with the anticipated square root dependence for diatomic gas.

OCIS codes: (120.4630) Optical inspection; (180.3170) Interference microscopy; (120.5050) Phase measurement; (240.6648) Surface dynamics; (160.3900) Metals.

References and links

1. T. Hübert, L. Boon-Brett, G. Black, and U. Banach, "Hydrogen sensors – A review," Sens. Actuators B Chem. **157**(2), 329–352 (2011).
2. B. G. Griffin, A. Arbabi, A. M. Kasten, K. D. Choquette, and L. L. Goddard, "Hydrogen detection using a functionalized photonic crystal vertical cavity laser," IEEE J Quantum Elect **48**(2), 160–168 (2012).
3. B. G. Griffin, A. Arbabi, and L. L. Goddard, "Engineering the sensitivity and response time of edge-emitting laser hydrogen sensors," Sensors Journal, IEEE **13**(8), 3098–3105 (2013).
4. M. A. Butler, "Optical fiber hydrogen sensor," Appl. Phys. Lett. **45**(10), 1007–1009 (1984).
5. M. A. Butler, "Micromirror optical-fiber hydrogen sensor," Sens. Actuators B Chem. **22**(2), 155–163 (1994).
6. J. Villatoro and D. Monzón-Hernández, "Fast detection of hydrogen with nano fiber tapers coated with ultra thin palladium layers," Opt. Express **13**(13), 5087–5092 (2005).
7. S. McKeown and L. Goddard, "Hydrogen detection using polarization diversity via sub-wavelength fiber aperture," IEEE Photonics **4**(5), 1752–1761 (2012).
8. A. Cusano, M. Consales, A. Crescitelli, and A. Ricciardi, *Lab-on-Fiber Technology* (Springer, 2015).
9. N. Liu, M. L. Tang, M. Hentschel, H. Giessen, and A. P. Alivisatos, "Nanoantenna-enhanced gas sensing in a single tailored nanofocus," Nat. Mater. **10**(8), 631–636 (2011).
10. A. Mandelis and J. A. Garcia, "Pd/PVDF thin film hydrogen sensor based on laser-amplitude-modulated optical-transmittance: dependence on H2 concentration and device physics," Sens. Actuators B Chem. **49**(3), 258–267 (1998).
11. M. Raval, S. McKeown, A. Arbabi, and L. L. Goddard, "Palladium Based Fabry-Pérot Etalons for Hydrogen Sensing," (Optical Society of America2012), p. STh2B.5.
12. I. P. Jain, Y. K. Vijay, L. K. Malhotra, and K. S. Uppadhyay, "Hydrogen storage in thin film metal hydride—a review," Int. J. Hydrogen Energy **13**(1), 15–23 (1988).
13. T. Flanagan and W. A. Oates, "The pallaium-hydrogen system," Annu. Rev. Mater. Sci. **21**(1), 269–304 (1991).

14. B. Ingham, M. F. Toney, S. C. Hendy, T. Cox, D. D. Fong, J. A. Eastman, P. H. Fuoss, K. J. Stevens, A. Lassesson, S. A. Brown, and M. P. Ryan, "Particle size effect of hydrogen-induced lattice expansion of palladium nanoclusters," Phys. Rev. B **78**(24), 245408 (2008).
15. T. N. Veziroğlu and S. Şahin, "21st Century's energy: Hydrogen energy system," Energy Convers. Manage. **49**(7), 1820–1831 (2008).
16. E. Wicke, H. Brodowski, G. Alefeld, and J. Völkl, "Hydrogen in metals II," Top. Appl. Phys. **29**, 258 (1978).
17. M. Wang and Y. Feng, "Palladium-silver thin film for hydrogen sensing," Sens. Actuators B Chem. **123**(1), 101–106 (2007).
18. F. Yang, D. K. Taggart, and R. M. Penner, "Fast, sensitive hydrogen gas detection using single palladium nanowires that resist fracture," Nano Lett. **9**(5), 2177–2182 (2009).
19. N. Krishna Mohan and P. K. Rastogi, "Recent devlopments in interferometry for microsystems metrology," Opt. Lasers Eng. **47**(2), 199–202 (2009).
20. C. Edwards, A. Arbabi, G. Popescu, and L. L. Goddard, "Optically monitoring and controlling nanoscale topography during semiconductor etching," Light Sci Appl **1**(9), e30 (2012).
21. G. Popescu, ed., *Quantitative Phase Imaging of Cells and Tissues* (McGraw-Hill, 2011).
22. C. Edwards, R. Zhou, S.-W. Hwang, S. J. McKeown, K. Wang, B. Bhaduri, R. Ganti, P. J. Yunker, A. G. Yodh, J. A. Rogers, L. L. Goddard, and G. Popescu, "Diffraction phase microscopy: monitoring nanoscale dynamics in materials science [Invited]," Appl. Opt. **53**(27), G33–G43 (2014).
23. C. Edwards, K. Wang, R. Zhou, B. Bhaduri, G. Popescu, and L. L. Goddard, "Digital projection photochemical etching defines gray-scale features," Opt. Express **21**(11), 13547–13554 (2013).
24. C. Edwards, A. Arbabi, B. Bhaduri, R. Ganti, P. J. Yunker, A. G. Yodh, G. Popescu, and L. L. Goddard, "Measuring the non-uniform evaporation dynamics of sprayed sessile microdroplets with quantitative phase imaging," Submitted (2014).
25. R. Zhou, C. Edwards, A. Arbabi, G. Popescu, and L. L. Goddard, "Detecting 20 nm wide defects in large area nanopatterns using optical interferometric microscopy," Nano Lett. **13**(8), 3716–3721 (2013).
26. B. Bhaduri, C. Edwards, H. Pham, R. Zhou, T. H. Nguyen, L. L. Goddard, and G. Popescu, "Diffraction phase microscopy: principles and applications in materials and life sciences," Adv. Opt. Photon. **6**(1), 57–119 (2014).
27. H. V. Pham, C. Edwards, L. L. Goddard, and G. Popescu, "Fast phase reconstruction in white light diffraction phase microscopy," Appl. Opt. **52**(1), A97–A101 (2013).
28. S. K. Debnath and Y. Park, "Real-time quantitative phase imaging with a spatial phase-shifting algorithm," Opt. Lett. **36**(23), 4677–4679 (2011).
29. C. Edwards, B. Bhaduri, B. G. Griffin, L. L. Goddard, and G. Popescu, "Epi-illumination diffraction phase microscopy with white light," Opt. Lett. **39**(21), 6162–6165 (2014).
30. S. F. Silva, L. Coelho, O. Frazao, J. L. Santos, and F. X. Malcata, "A Review of Palladium-Based Fiber-Optic Sensors for Molecular Hydrogen Detection," Sensors Journal, IEEE **12**(1), 93–102 (2012).
31. Y. Morita, K. Nakamura, and C. Kim, "Langmuir analysis on hydrogen gas response of palladium-gate FET," Sens. Actuators B Chem. **33**(1-3), 96–99 (1996).
32. T. P. Leervad Pedersen, C. Liesch, C. Salinga, T. Eleftheriadis, H. Weis, and M. Wuttig, "Hydrogen-induced changes of mechanical stress and optical transmission in thin Pd films," Thin Solid Films **458**(1-2), 299–303 (2004).

1. Introduction

Before hydrogen fuel cell technology can become practical for energy production or storage, reliable sensors must be developed to detect H_2 well below the lower explosive limit of 4% in air. A popular subset of H_2 sensors use Pd, which reacts readily with H_2 and produces optical, electrical, and structural changes that result in several detection mechanisms [1]. Some of these include functionalized waveguides or lasers where the lasing conditions are altered [2, 3], optical fiber sensors [4–8], plasmonic devices [9], and transmission/reflection monitoring of thin films [10, 11]. While the optical and electrical changes are well understood, much less is known about the structural changes. In this paper, we investigate the H_2 induced axial expansion of Pd microdisks, to better characterize the nanoscale structural changes, which can be used to simulate new sensor designs. There have been many studies on the PdH system for bulk materials [12, 13], and more recently on nanoparticles [14], but few studies have been done on nano and microscale structures that are typically used for sensing applications.

2. Physical mechanism

When gaseous H_2 molecules come in contact with Pd, they disassociate into single atoms and diffuse into the face-centered cubic (FCC) Pd lattice. The H atoms bond to the interstitial sites and form PdH, which starts in the α-phase (low concentration), where the process is completely reversible. Once the H_2 concentration reaches the lower critical limit α_{max}, regions containing PdH begin to swell forming β regions and the film enters an α + β phase, as the two are immiscible at standard temperature and pressure [13]. When the H_2 concentration is

increased above the upper critical limit β_{min}, the Pd will consist entirely of β regions. Values of α_{max} and β_{min} can vary drastically depending on the film thickness and the method and angle of deposition. The forming of β regions is referred to as hydrogen induced lattice expansion (HILE), where the lattice constant can increase up to 3.5% [13] since Pd can absorb up to 900 times its volume in hydrogen [15]. This expansion is highly isotropic due the symmetry of available bonding sites for hydrogen within the FCC lattice structure of Pd [13]. When the Pd is weakly bonded to the substrate, such as with a quartz substrate, the isotropic expansion can lead to micro-blistering, micro-cracking, and buckling of the Pd film [4, 5]. Fortunately, these changes and also lattice expansion are reversible, at least for some time at low concentrations [4, 5]. However, at higher H_2 concentrations, the transition to the β phase can induce plastic deformations, resulting in permanent structural changes. Evidence of the β phase can be seen at about 1.5% H_2 for our films. In practice, a high volume of repeated exposures or even a single prolonged exposure at a high enough concentration can lead to film embrittlement or delamination [16, 17]. In general, the sensitivity, response time, and recovery time of a Pd sensor that undergoes structural changes will depend on the surface adhesion, substrate material, film thickness, method of deposition, and the geometry of the sensor.

For electrical sensors, the introduction of hydrogen into the lattice changes the carrier concentration and mobility which leads to changes in conductance [18]. For optical sensors, hydrogen atoms that bond at the interstitial sites serve as electron donors which results in orbital hybridization with the 4d band of the Pd atoms and a change in the Fermi level. This alters the optical transition rate and thus changes both the real and imaginary parts of the refractive index [10, 13, 16]. These refractive index changes can be readily detected using many approaches [1, 2, 4, 5, 7, 11, 13]. Hydrogen absorption also results in structural changes in the Pd, which are much more difficult to measure and not well documented for thin films or microstructures. A sensitive technique is required to measure the nanoscale changes during H_2 exposure. Recent advances in quantitative phase imaging (QPI) provide a solution for this challenge [19–22]. To monitor changes in situ, we applied epi-illumination diffraction phase microscopy (epi-DPM), a reflection-geometry QPI method. Epi-DPM is a proven technique with sub-nanometer height measurement accuracy; it has been used to monitor wet etching of semiconductors [20], photochemical etching [20, 23], microdroplet evaporation [24], and material deformation, as well as to detect defects in patterned semiconductor wafers [25].

3. Experimental setup and sample preparation

The setup is shown in Fig. 1. Epi-DPM uses a 532 frequency-doubled Nd-YAG laser, diffraction grating, 4f lens system, spatial filter, and charge-coupled device (CCD) camera (Zeiss AxioCam MRm) to realize a compact Mach-Zehnder interferometer which produces an interferogram at the CCD. To obtain the complex analytic signal and phase associated with our measured interferogram, we perform a spatial Hilbert transform. Numerically, we bandpass filter (BPF) the measured signal, bring it back to baseband, extract the phase, and reconstruct the surface topography with sub-nanometer accuracy [26]. Epi-DPM is a single-shot non-destructive method that does not require staining or coating of the specimen. This unique collection of features enables the epi-DPM system to accurately monitor nanoscale dynamics in their natural environment. Additional details about the DPM and epi-DPM methods and phase retrieval can be found in several references [20, 22, 26–29].

Phase is much more sensitive than amplitude to the topography of the sample. As fields from the source interact with the sample, phase shifts are induced in the scattered light with respect to the unscattered light. These changes in the optical path length contain the desired structural information. The method is both sensitive and stable and provides topographic height information with 0.55 nm spatial (i.e., point to point) and 0.43 nm temporal (frame to frame) sensitivity [20, 23]. Note that averaging over a portion of the image spatially, or over a collection of frames temporally, can further reduce the noise. Both forms of averaging will be used in our analysis of the axial expansion of the Pd microdisks.
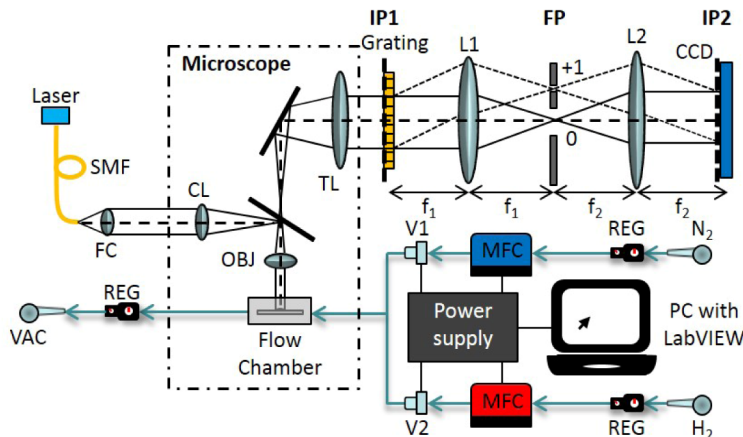
Fig. 1. Experimental setup. Epi-DPM was used to monitor height changes to the Pd microdisk sample housed in a flow chamber with H_2 and N_2 rates set via LabVIEW. *Abbreviations: SMF, single mode fiber; FC, fiber collimator; CL, collector lens; OBJ, objective; TL, tube lens; L1/L2, lenses; V1/V2, valves; MFC, mass flow controller; REG, regulator; VAC, vacuum line.*

An aluminum flow chamber was custom-built to hold the samples, which contains a transparent imaging window placed at a small 7° angle to prevent multiple reflections. The flow cell had a 32 mm x 19 mm base, 5mm left height, 9mm right height, and a total volume of $4.25x10^3$ mm^3. Regulators and mass flow controllers were used to control the pressure and gas flow of H_2 and N_2 via LabVIEW. Valves were also used to keep the lines charged so that diffusion of the gas from the source did not add delay or affect the H_2:N_2 pulse shape.

Pd microdisks on quartz (SiO_2) substrates were fabricated using e-beam evaporation and a shadow mask. SiO_2 is of particular interest due to its extensive use in fiber-based H_2 sensing applications [7, 30]. Poor substrate adhesion prohibited the use of standard lithography and lift-off techniques without. The shadow mask has 180 μm diameter holes with a 350 μm pitch and was placed very close to the substrate. As shown in Fig. 2(a), a 260 nm Pd layer was deposited, the shadow mask was removed, and 40 nm of Pd was blanket deposited. The blanket deposition of this optically thick Pd layer ensures that both the microdisks and the background have the same complex refractive index, which allows changes in the microdisk height to be decoupled from changes in the reflection coefficient's phase due to changes in the complex refractive index of the Pd layer. Variable angle spectroscopic ellipsometry (VASE) data yielded a complex refractive index of 1.56 + 3.64j for our Pd structures. Furthermore, the shadow mask approach creates smoother edges, which prevents phase unwrapping errors in our measurements [26]. Note that the blanket deposition was also masked with a straight edge of Kapton tape to allow us to verify the thicknesses of the blanket layer. See Fig. 2(b).
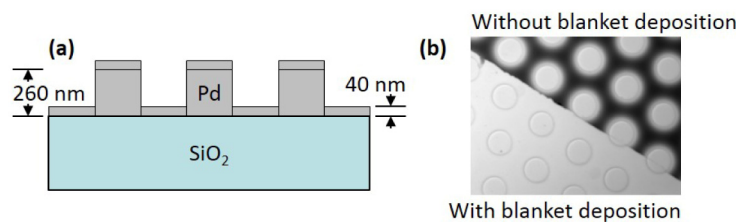

Fig. 2. Pd microdisk sample. (a) Schematic of 260 nm tall Pd microdisks on a quartz substrate and the 40 nm blanket deposition. (b) Bright-field image shows an edge of the blanket.

4. Experimental results

Figure 3(a) shows the surface topography of a Pd microdisk and its initial dimensions. The initial height relative to the background before H_2 exposure was 264.4 nm and the full width
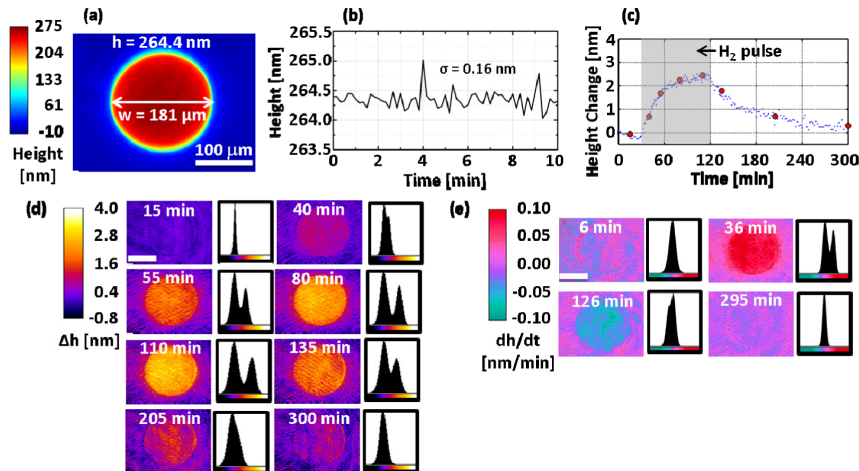
Fig. 3. Differential height measurements during H_2 exposure. (a) Height map of a Pd microdisk before H_2 exposure using epi-DPM. (b) Stability of height measurement during N_2 baseline run. (c) Average height change of the Pd microdisk. H_2 was turned on to 0.4% at 30 min and turned off at 120 min. (d) Selected frames and their histograms for the local height change at various times indicated in (c). (e) Instantaneous expansion rate before exposure, during expansion, during recovery, and after recovery. All scale bars are 100 μm.

at half maximum was 181 μm. The height was measured by averaging over a circular region containing the top flat portion of the microdisk. Figure 3(b) shows the temporal stability of the system during an N_2 calibration run. The temporal noise for the mean microdisk height in the presence of 300 standard cubic centimeters per minute (sccm) of N_2 flow was 0.16 nm.

Figure 3(c) shows the change in microdisk height versus time for a 0.4% H_2 pulse. An initial 30 min baseline was acquired using pure N_2 at 300 sccm. H_2 was then switched on and the flow rates were adjusted to maintain the 300 sccm total rate. The H_2 ran for 90 min and was shut off at the 120 min mark. The chamber was then purged with pure N_2 at 300 sccm for 3 hours. Frames were acquired every 6 s during pure N_2 exposure and every 3 s during the H_2 pulse. During the experiment, the sample drifted very slightly, on the order of 100 nm in the sample plane or ½ of a CCD camera pixel at the image plane. To obtain the most accurate instantaneous height change images, this in-plane motion was corrected by registering the epi-DPM height images with sub-pixel resolution as follows. First, each frame of the 30 min N_2 baseline was registered by performing a cross-correlation with the very first frame, finding the position of maximal cross-correlation r_{max} with sub-pixel precision by fitting the cross-correlation image with a 2nd order polynomial in the neighborhood of its largest value, and then linearly interpolating the epi-DPM height image onto a grid that is shifted by -r_{max}. After registration, these baseline epi-DPM images were averaged to reduce noise and thereby produce the most accurate baseline image against which to compute the instantaneous height change. Next, each image of the entire pulse test was registered to this baseline image and the instantaneous height change images were computed by subtraction. To reduce temporal noise, these instantaneous height change images were then averaged for 1 min, i.e. 10 frames during the N_2 exposures and 20 frames during the H_2 pulse. The axial expansion of the microdisk is thereby measurable in a spatially and temporally resolved manner with very high accuracy.

Figure 3(d) shows instantaneous height change images of the microdisk during the pulse test and their associated histograms, where the frames were selected from Fig. 3(c) to evenly sample the axial expansion process. The expansion can be clearly observed in Fig. 3(d) as the initial histogram peak with zero height splits into two peaks during H_2 exposure, one remaining at a height of zero while the other revealing the expansion, and subsequently the peaks merge back into a single one upon purging the chamber with N_2. Furthermore, small deformations, or local heterogeneities, can be observed during parts of the expansion and

recovery process. These are observed in the histogram by considering the width of the peaks, but are more easily identifiable in the instantaneous height change images.

Figure 3(e) shows a select subset of the spatially and temporally resolved instantaneous rate of axial expansion at four key moments: before exposure (6 min), at the beginning of expansion (36 min), at the beginning of recovery (126 min), and far into recovery (295 min). For best accuracy, the instantaneous axial expansion rate images were computed pixel by pixel by performing a simple linear regression of the height change versus time for a 10 min window centered at the times specified in Fig. 3(e). From these images, we see a negligible expansion rate before exposure and far into recovery and about a 0.1 nm/min expansion rate at the onset of H_2 exposure and a 0.1 nm/min contraction rate as the H_2 is turned off. Further, the expansion and contraction rates are relatively uniform across the Pd microdisk.

The standard pulse test was repeated for other H_2 concentrations to be able to quantify the dependency of axial expansion on concentration. Figure 4(a) shows the height changes for the various pulse tests. The response times were all approximately 30 min. After recovering in N_2, the height returned to its initial value to within the noise of the system. The recovery time was approximately 2-3 hours for all cases. Figure 4(b) shows the change in height in percent, Δh, for each pulse test as a function of the H_2 concentration in percent, c. For ideal films at constant temperature, the axial expansion process is limited by surface adsorption which is governed by either the Langmuir or Freundlich isotherms [31]. Given the low adsorbate concentrations used in this study, the Freundlich equation is more appropriate. Assuming that the axial expansion is linear with PdH content, this power law fit can be applied to the percent height change data [31]. This provides a model for the microdisk height change $\Delta h(c) = k \cdot c^n$. Fitting the data to a power law gives $k = 1.28 \pm 0.06$ and $n = 0.51 \pm 0.04$, which agrees well with Sievert's Law ($n = 0.5$) and the anticipated square root dependence for diatomic gas [32].
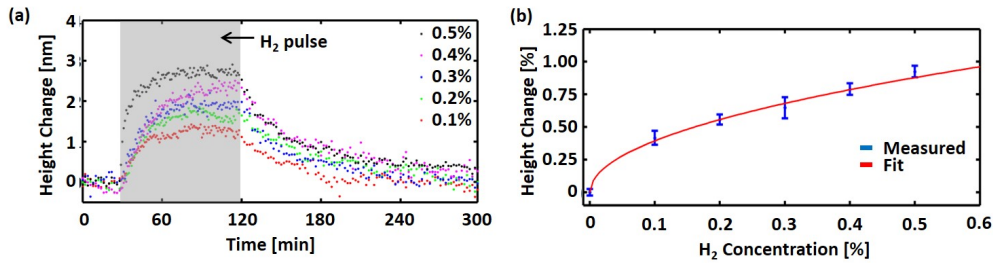

Fig. 4. H_2 induced height changes of a Pd microdisk. (a) Measured height change for different H_2 concentration pulse tests. (b) Percent change in height, Δh, versus percent H_2 concentration, c, with Freundlich fit: $\Delta h(c) = k \cdot c^n$, where $k = 1.28 \pm 0.06$ and $n = 0.51 \pm 0.04$.

5. Conclusions

We have demonstrated a method to monitor the nanoscale axial expansion in Pd microdisks during H_2 exposure. The noise floor of the height measurement during gas flow was 0.16 nm without temporal averaging. The quantitative phase imaging method enabled us to determine the axial expansion coefficient as a function of H_2 concentration and verify its fit to a power law agreed with Sievert's Law. Further, the very low noise floor of the technique combined with appropriate averaging and simple linear regression enabled us to quantify the axial expansion rate in a spatially and temporally resolved manner. We anticipate that these new measurement capabilities will lead to the development of new classes of sensors across various fields that are based on nanoscale structural changes.

Acknowledgments